Journal of Materials Chemistry A

Accepted Manuscript

ROYAL SOCIETY OF CHEMISTRY

www.rsc.org/materialsA

Journal Name

ARTICLE

1-D Oriented Cross-Linking Hierarchical Porous Carbon Fibers as Sulfur Immobilizer for High Performance Lithium-Sulfur Batteries†

Received 00th January 20xx,
Accepted 00th January 20xx

DOI: 10.1039/x0xx00000x

www.rsc.org/

Xiaofei Yang‡[a,b], Ying Yu‡[a,b],Na Yan[a,b], Hongzhang Zhang*[a], Xianfeng Li[a,c] and Huamin Zhang*[a,c]

One-dimensional (1D) oriented cross-linking hierarchical porous carbon fibers (CHPCF) was first designed and proposed as the sulfur immobilizer for lithium–sulfur (Li-S) batteries application. The CHPCF owns large length/diameter (L/D) ratio, cross-linked structure and reasonable hierarchical porous distribution, which provides "green channels" for both e^- and Li^+ transport. Besides, the CHPCF possesses large micro-porous surface to confine the polysulfide (PS) diffusion. As a result, the S/CHPCF cathodes simultaneously achieve excellent C-rate performance and cycling stability, which is 535 mA h g^{-1} at 15C (1C = 1672 mA g^{-1}) and 0.076 % capacity attenuation per cycle at 5C during 500 cycles. The structure-performance relationship of the carbon materials and Li-S batteries was studied in detail. This research work would shed light on the materials design of Li-S batteries with excellent C-rate performance.

Introduction

Exploration and development of such power-intensive applications as long-range electrical vehicles and stationary energy storage leads to strong demand for advanced rechargeable batteries, especially on the aspects of specific capacity and energy density.[1-4] As one of the most promising candidates, Li-S batteries are well-suited due to the superior theoretical specific capacity of 1675 mAh g^{-1} and energy density of 2600 Wh kg^{-1}, based on electrochemical reaction between sulfur and lithium ($16Li + S_8 \leftrightarrow 8Li_2S$).[1, 5-7] What's more, sulfur, one of the most abundant elements in the earth's crust, as well as being cost-effective and environmental friendly, make them stand out from tremendous rechargeable batteries and offering the possibility for their practical application.[1, 2, 8-12] Nevertheless, behind the towering merits, still series of critical issues like the insulating nature of sulfur and Li_2S_2/Li_2S, serious volumetric expansion during sulfur lithiation and "shuttle effect" arising from PS "shuttle" between the cathode and anode, co-lead to such inferior electrochemical performance as low capacity, low coulombic efficiency and fast capacity-fading.[2, 13] To echo to these considerable challenges, tremendous efforts have been focused on confining the sulfur species with advanced porous frameworks to improve the electrochemical performance of Li-S batteries.[3-5, 13-24]Among them, hierarchical porous carbon (HPC) powder with multi-scale pores have attracted most attention and achieved impressive progress on capacity output and cycling stability under low C-rates. [14, 16, 25-28] For instance, we have already developed soft-package Li/S battery with high energy density up to 504 Wh kg^{-1} with S/HPC based cathode materials, while the operating C-rate was as lower as 0.01C and quite insufficient for EV application.[29]

Is that possible to increase the C-rate over 5C or even higher, to compete with the commercial Li-ions batteries such as $LiFePO_4$ and NCM? In order to achieve this goal, both the Li^+ and e^- transport speed inside the cathode should be further enhanced, which could be separately realized by tuning the pore distribution from micro to macro and by adding more nano-scale conductive carbon materials (carbon black, CNT, graphene). The e^- transport frameworks, however, are simply formed "through point contacting" electron transfer mode between carbon, with the e^- conductive speed limited at the carbon /carbon interface. In worse conditions, the active composites (S/C) might even be isolated by binders, if the carbon materials were not sufficiently contacted with each other., especially when impregnating a large quantity of sulfur.[20, 21, 30, 31] In previous research works, the 1D oriented carbon materials shows generally appealing C-rate performance in Li-S batteries. Then an interesting conception comes out: if we cross-link (or joint) these 1D carbon materials together with 1D carbon materials, the e^- conductivity would be further improved. Besides that, if the 1D carbon also owns excellent porous structure (large pore volume and surface area), both the C-rate performance and cycle stability of Li-S batteries would be much improved.

Based on this consideration, MOF was chosen as the precursor to obtain this carbon structure. As is well known, MOF is a well-organized framework constructed with metallic ions and organic ligands, which may remain the previous morphology and porous structure after carbonizing under high temperature.[32] For example,

[a] Division of Energy Storage, Dalian Institute of Chemical Physics, Chinese Academy of Sciences, Zhongshan Road 457, Dalian 116023, China; E-mail: zhanghz@dicp.ac.cn; Fax:+86-411-84665057; Tel.:+86-411-84379669
[b] University of Chinese Academy of Sciences, Beijing 100039, China
[c] *Collaborative Innovation Center of Chemistry for Energy Materials (iChEM), Dalian 116023 (P.R. China)*
† Electronic Supplementary Information (ESI) available: [details of any supplementary information available should be included here]. See DOI: 10.1039/x0xx00000x
‡ Xiaofei Yang and Ying Yu contributed equally to this work.

we noticed that the carbonization of micro-porous MOF precursor would mainly obtain micro-porous carbon material. What's more, the metallic ions might be reduced to corresponding metal or metallic oxides that act as "localized" inner templates to form meso-pores. Additionally, the macro-pores could be formed due to the synergic effect of organism decomposition and gas activation during carbonization. Given this, the desired 1D oriented carbon fibers with hierarchical pores could be obtained by carbonizing the 1D MOF fibers, and cross-linking with each other via organisms melting and carbonizing under high temperature. Along this line, inspired by our early work,[33] a cross-linked hierarchical porous carbon fibers (CHPCF) with one-dimensional (1D) orientation and mutil-scale pore distribution was fabricated from a well-designed Cu-MOF with unique morphology and applied as sulfur host material. As expected, the Li-S batteries assembled with S/CHPCF composite cathode show excellent cycling stability and C-rate performance. The detailed material preparation and structure-performance relationship of CHPCF was systemically studied, as well as compared with the uncross-linked 3D MOF based carbon materials which were manufactured with the same raw materials.

Results and discussion

The 1D MOF with high length/diameter (L/D) ratio, comparable to commercial nanotubes and nanofibers (L/D>1000), was designed as precursor to prepare CHPCF as the sulfur immobilizer to supply Li^+ /e^- with "green channel". The whole synthesis process was illustrated in Fig. 1. First, the 1D ordered Cu-MOF fibers, assigned to $[Cu(BTC–H_2)_2\text{-}(H_2O)_2]\cdot 3H_2O$ phase (labeled as Cu-BTC here) as reported,[34] with diameter of nearly 200 nm were synthesized for the first time by coordinating copper ion (Cu^{2+}) with benzene-1,3,5-tricarboxylic acid (BTC) under hydrothermal atmosphere (see Supporting Information, Fig. S1). For comparison, the Cu-MOF with the same raw materials but different morphology (10 µm octahedral type, assigned to $Cu_3(BTC)_2$, also known as HKUST-1) was also synthesized (Fig. S2) according to S. I. D. Williams's group in a water/ethanol mixture.[35] The structures of Cu-BTC and HKUST-1 were determined by the XRD and FTIR curves, [34] as shown in Fig. S3.

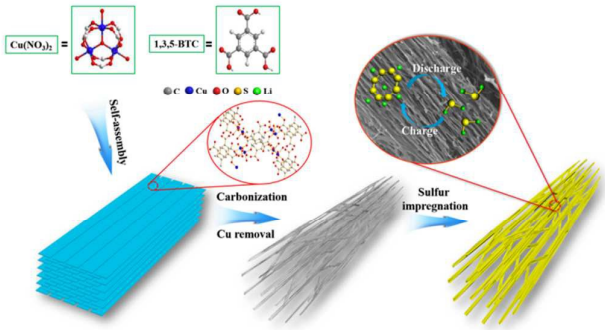

Fig. 1. Scheme of S/CHPCF preparation.

Interestingly, after carbonization (the sample labled as Cu-BTC-C), as shown in Fig. S4, the fibers cross-linked with each other forming the cross-linking fibrous structure. Besides, a large number of residual nanoparticles (20 nm in diameter) were found to be coated on the backbone of the fibers with a few layers of graphitic carbon (Fig. S4d). The particles are mainly identified as metallic copper (Cu) by the high-resolution TEM image, with lattice fringes of ~0.21 nm periodicity, which is consistent with the (111) plane of the fcc phase metallic Cu.[36, 37] The XRD pattern can further support this deduction, with two sharp peaks of Cu(111) and Cu(200) appeared at 44° and 51° (Fig. S5). In addition, two peaks at 37° and 62° corresponding to Cu_2O(111) and Cu_2O (220) suggsts that partial Cu was transformed into Cu_2O by slow oxidation in air.[37] However, both Cu and Cu_2O particles would bring down the specific surface area and pore volume of carbon materials (Cu-BTC-C: 172 $cm^2\ g^{-1}$, 0.15 $cm^3\ g^{-1}$, Fig. S6), which would hinder the Li-S battery performance. In order to remove all of the residue particles, the carbon shells coated on the nanoparticles were firstly broken with KOH activation and then the nanoparticles were washed with HNO_3 aqueous solution. After removing the particles, the CHPCF maintained the ordered cross-linking fibrous structure with length up to hundreds of micrometers (Fig. 2a-c), and a large amounts of meso-pores around 20 nm appeared (Fig. 2d-f). As further confirmed with the EDX results (inset of Fig. 2c), the peaks corresponding to Cu (inset of Fig. S4b) also vanished. The unique structure is suitable for Li-S batteries with high C-rate, because the macro-pores among the ordered fibers and the meso-pores in fibers can facilitate Li^+ transportation as well as large surface area for electrochemical reaction.[14] Additionally, the 1D oriented carbon fibers are crosslinked with carbon, which effectively eliminate the contact resistance between the fibers. Due to the synergetic merits in facilitating Li^+ and e^- transportation, an excellent C-rate performance for the Li-S batteries assembled with CHPCF can be expected. In comparison, the carbon derived from HKUST-1 (named as HKC), another MOF prepared with the same raw materials with HPCF, shows a morphlogy of deformed octahedron (Fig. S7a-c) with size of nearly 10 µm after the same treatment. Even though HKC also owns numerous hierarchical pores, its Li^+ transportation distance is much longer (10 um vs. 100 nm) than the CHPCF and the "throug point contacting" electron transfer model will harmper the e^- transportation, which limit the C-rate performance of Li-S batteries.

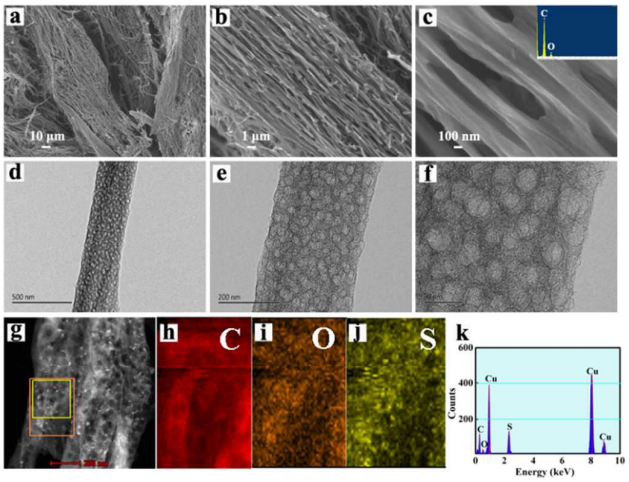

Fig. 2. (a) ~(c) SEM images (inset of c is EDX pattern) and (d) ~ (f) TEM images of CHPCF at differnet magnifications. (j) STEM images of S/CHPCF and elemental mapping of (h) carbon, (i) oxygen and (j) sulfur. (k) EDX of S/CHPCF.

The N_2 adsorption-desorption isotherm and pore size distribution were used to quantitatively analyze the porous structure of the hosts. As analyzed via Barrett-Joyner-Halenda (BJH) method, the HKC shows a micro-pore distribution and a broadened distribution from 30-200 nm, while the CHPCF shows a micro-pore distribution and a relatively narrow meso-pore distribution around 20 nm (Fig. 3b). It is noteworthy that the micro-pores of CHPCF are more than those of HKC, which are beneficial for confining soluble PS during cycling.[21] Due to the abundant micro-, meso- and macro-pores, both carbons deliver high specific surface areas and large pore volumes (HKC : 1623 $m^2 g^{-1}$, 1.13 $cm^3 g^{-1}$; CHPCF: 1906 $m^2 g^{-1}$, 1.35 $cm^3 g^{-1}$, Fig. 3c). After 60 wt. % sulfur impregnation, the specific surface area and pore volume of obtained S/C composites decreased seriously (S/HKC: 16 $m^2 g^{-1}$, 0.15 $cm^3 g^{-1}$; S/CHPCF: 12 $m^2 g^{-1}$, 0.06 $cm^3 g^{-1}$), suggesting that sulfur successfully impregnated into the pores.[3] Besides, nearly all micro- and meso-pores disappeared and only partial macro-pores remained for accommodating volume expansion. All in all, CHPCF owns not only unique morphology but also optimized hierarchical porous structure for Li-S batteries application.

To understand the state of sulfur in the hosts after a heating process at 155 °C for 20 hours, the crystal structure was analyzed by X-ray diffraction (XRD). As presented in Fig. 3d, the S/C composites show a similar XRD pattern to the hosts, with no characteristic peaks of crystalline sulfur but only one broadened peak around 25 ° corresponding to (002) plane of amorphous carbon. It's speculated that most sulfur was confined into the host or uniformly dispersed in amorphous state of carbon surface,[33, 38] as further confirmed via STEM and elements analysis (in Fig. 2g-k and Fig. S7d-h).

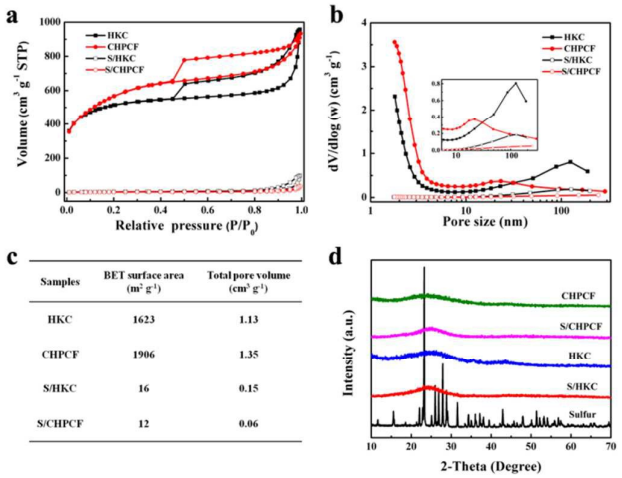

Fig. 3. (a) Nitrogen adsorption—desorption isotherms, (b) Pore size distribution curves and (c) Physical characteristics of HCK, S/HKC, CHPCF and S/CHPCF composites.(d) XRD patterns of orthorhombic S, HKC, S/HKC, CHPCF and S/CHPCF composites.

The cycling performance of the cells assembled with S/HKC and S/CHPCF cathodes was studied at C-rates of 1C and 5C between 1.0 V and 2.8 V in a $LiNO_3$-free electrolyte. As illustrated in Fig. 4a, the cell assembled with S/CHPCF can still deliver a high initial discharge capacity of 1336 mA h g^{-1} at 1C, equaling to 80% of the theoretical capacity (1672 mA h g^{-1}), which is much higher than the 1181 mA h g^{-1} of S/HKC electrode. Besides, after 100 cycles, the S/CHPCF cathode still remains a high capacity of 904 mA h g^{-1} (68% of the initial discharge capacity), which is 1.5 times of that of S/HKC cathode (599 mA h g^{-1}, 51% of the initial discharge capacity). When the C-rate was increased to 5C, the difference was enlarged. For example, the initial discharge capacity and the residual capacity after 100 cycles of the cell assembled with S/CHPCF electrode are 1032 mA h g^{-1} and 680 mA h g^{-1}, while the relevant values of S/HKC electrode are only 614 mA h g^{-1} and 360 mA h g^{-1}. The excellent active mass utilization and retention can be attributed to two factors: 1) larger proportion of micro-pores can not only provide sulfur with large carbon surface to connect with but also limit the soluble PS diffusion via strong capillary force. It can be further confirmed by self-discharge test. As shown in Fig. S8, the cell assembled with S/CHPCF electrode can deliver a high capacity of 770 mA h g^{-1} after the cell was first discharged to 400 mA h g^{-1} (the concentration of PS is the highest at this period) and then rested for 100 h at 0.5C, whereas the S/HKC electrode only delivered a capacity of 497 mA h g^{-1}; 2) the fluffy structure of CHPCF (Fig. S9a) can provide more space to accommodate electrolyte. Even though a large amount of pores were filled with sulfur, the S/CHPCF electrode still shows nearly 1.8 times of electrolyte uptake compared to S/HKC electrode (S/CHPCF: 559 wt%, S/HKC:316wt%, Fig. S9b), which means that more soluble PS can be maintained and utilized in host. The enlarged difference with C-rate increasing might result from polarization effect, which will be discussed in the section of C-rate performance in detail. In common consideration, with the discharge cutoff voltage increasing, the cycling stability improves gradually due to the relieved sluggish reaction arising from the poor electric conductivity and slow diffusion of insoluble Li_2S_2/Li_2S.[39] Hence, the cycling performance of S/HKC and S/CHPCF was further investigated between 1.7 V and 2.8 V with $LiNO_3$ as additive to confine the self-discharge. As presented in Fig. 4c, the cell assembled with S/CHPCF electrode can achieve a high initial discharge capacity of 960 mA h g^{-1} and retain 57 % (547 mA h g^{-1}) after 500 cycles at 2C. When the C-rate was increased to 5C, a high initial capacity of 801 mA h g^{-1} was still achieved. Similar to previous reports,[40-42] the capacity decreased sharply during the first few cycles (nearly 70 cycles), due to the irreversible PS diffusion. Then, a reversible capacity of nearly 500 mA h g^{-1} (62% of the initial capacity) was remained, meaning that a low decay rate of 0.076% per cycle was obtained, which can be further testified by its charge/discharge curves in Fig. 4b. As can be seen, after 100 cycles, all charge and discharge curves are nearly overlapped. The excellent cycling performance can be ascribed to the high proportion of micro-pores, the diminished volumetric expansion effect and the passive layer coated on the Li anode that decreased the shuttle effect after $LiNO_3$ addition. To the best of our knowledge, this is the best Li-S batteries performance using MOF-derived carbons as the hosts.[26, 33, 38, 43-45] In comparison, the cell assembled with S/HKC electrode only shows initial discharge specific capacity of 849 mA h g^{-1} and 416 mA h g^{-1} at 2C and 5C, with low capacity retentions of 30% (257 mA h g^{-1}) and 39% (252 mA h g^{-1}) after 500 cycles, respectively. The obvious cycling performance difference further highlights the merits of the designed structure of CHPCF.

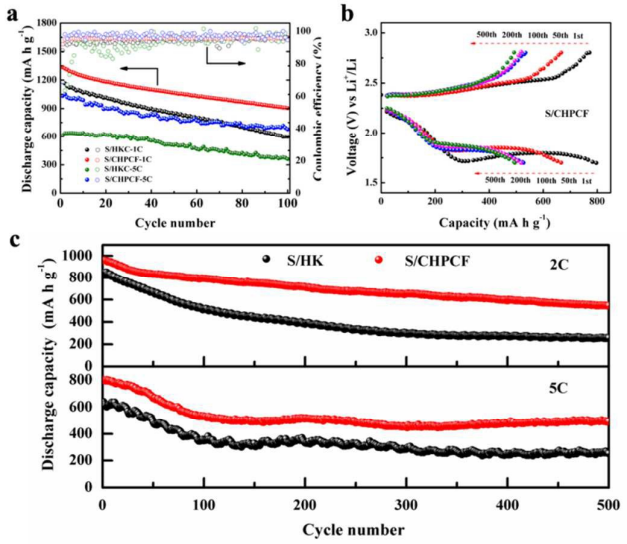

Fig. 4. (a) Cycling performance of S/HKC and S/CHPCF electrodes in a $LiNO_3$-free electrolyte. (b) Charge/discharge curvers of S/CHPCF electrode at 5C in the 1st, 50th, 100th, 200th and 500th cycles (the dates collected from Figure 4c). (c) Long-term cycling performance of S/HKC and S/CHPCF electrodes with $LiNO_3$ as additive.

To further illustrate the excellent cycling performance of S/CHPCF, an in-situ visual electrochemical experiment was carried out to show the interaction between PS and hosts, by observing the color change of the electrolyte in optically transport vessels (Fig. 5a) at corresponding discharge states (Fig. 5b). As shown in Fig. 5c, the colorless electrolyte (stage a) gradually changed to brown (stage b and c) as a result of the PS diffusing out of hosts. Interesting, when the cell was discharged from stage c to e, unlike the previous reports,[33, 46] the electrolyte color of HKC didn't shallow, which may be result from insoluble and poor conductive Li_2S_2/Li_2S coated on the surface or blocked the external pores of host that further hindered the PS to the internal active site due to the micron size of HKC. On the contrary, the electrolyte surrounding S/CHPCF electrode from stage a to e turn back to its initial color (Fig. 5d). Hence, the in-suit visible experimentation is highly consistent with the cycling performance of the batteries and further confirms the strong capability of CHPCF in confining the PS species.

The C-rate performance of S/HKC and S/CHPCF electrodes was investigated in Fig. 6. The discharge capacity would decrease under higher C-rate, attributed to an increased overpotential (overpotential mentioned here was calculated based on the potential difference between the charge plateau and the second discharge plateau). However, the increased trend of overpotential was more moderate for S/CHPCF electrode. Even the C-rate was increased to 5C, the overpotential of S/CHPCF electrode was only 490 mV, which was 210 mV smaller than that of S/HKC electrode (Fig. 6e), indicating a kinetically efficient reaction process with a small barrier.[9] Due to the smaller overpotential, more capacity can be output for S/CHPCF electrode, especially at high C-rates. The cell assembled with S/CHPCF electrode can deliver a capacity as high as 534 mA h g^{-1} at a high C-rate of 15C, which is twice more than that of the battery assembled with S/HKC electrode (259 mA h g^{-1}). The excellent C-rate performance can be ascribed to the ordered fibers with 1D orientation and macro-pores established between the ordered fibers and its branches in the unique cross-linking structure, which were helpful for e^- transportation and electrolyte infiltration/Li^+ transportation, respectively.

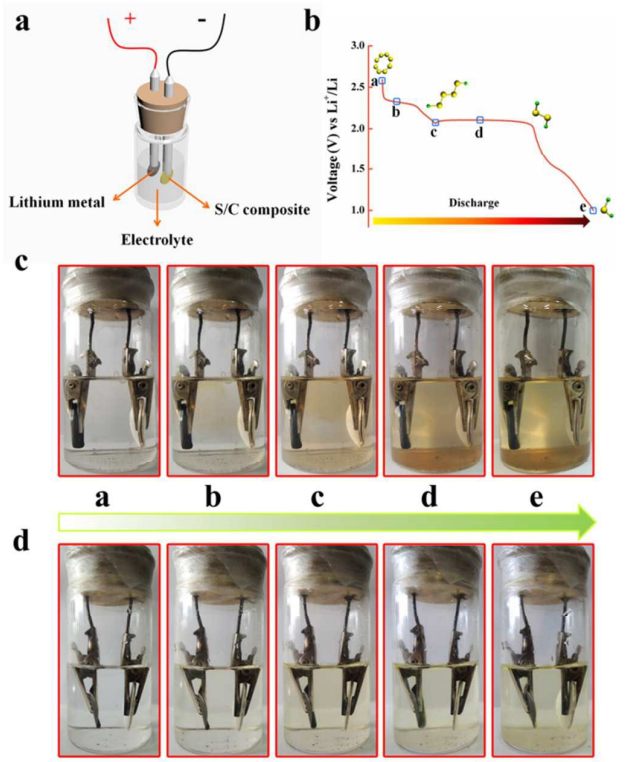

Fig.5. (a) Schematic illustration of visual–electrochemical study. (b) Schematic of a typical voltage profile. Visual confirmation of polysulfide entrapment of (c) S/HKC and (d) S/CHPCF cathodes at different states of discharge from stage a to e in (b) at a C-rate of 0.1C.

Two important parameters of U_1 and Q_2/Q_1 were introduced to further verify the speculation. According to the previous report and shown in Fig. 6f, U_1, the onset potential of the first discharge plateau at higher voltage, can reflect the interfacial kinetics between the host and active sulfur.[22] Q_0 is the theoretical capacity of 1672 mA h g^{-1}, including the discharge capacity plateau at higher voltage (Q_1) and the discharge capacity plateau at lower voltage (Q_2), as follows:

Plateau around 2.3 *V*:

$$S_8 + 4e^- \longleftrightarrow 2S_4^{2-}$$

$$Q_1 = 1/4Q_0, Q_0 = 1672\ mA\,h\,g^{-1}; \quad (1)$$

Plateau around 2.1 *V*:

$$2S_4^{2-} + (12 - 2n)e^- + (16 - 2n)Li^+ \longleftrightarrow nLi_2S_2 + (8 - 2n)Li_2S \quad (2)$$

$$Q_2 = (3/4 - n/8)Q_0,\ 0 \le n \le 4,\ 1 \le Q_2/Q_1 \le 3.$$

In theory, the plateau around 2.3 V has the potential to output a capacity of 418 mA h g^{-1}, equaling to 1/4 of theoretical capacity, due to 1/2 electron per sulfur atom transfer from sulfur to Li_2S_4. The plateau around 2.1 V can be ascribed to further reducing Li_2S_4 to Li_2S, equaling to 3/4 of theoretical capacity. However, during this process, insoluble Li_2S_2/Li_2S were produced, which greatly increased the resistance of Li^+/e^- transportation and further led to a low value of Q_2/Q_1. Hence, the value of Q_2/Q_1 is also regarded as a good indicator to evaluate the capability of Li^+/e transportation within

the host.[22] Fig. 6g-h exhibit the evolutions of U_1 and Q_2/Q_1 of S/HKC and S/CHPCF electrodes during C-rate increasing from 0.5C to 5C (when the C-rate was increased to more than 5C, the plateaus of S/HKC electrode become obscure. Hence, only U_1 and Q_2/Q_1 from 0.5C to 5C were given here.) It is not hard to see that both U_1 and Q_2/Q_1 decreased gradually with the C-rate increases, especially at high C-rates, which mainly results from polarization effect. Even though, no matter what C-rate is, both the U_1 and Q_2/Q_1 of S/CHPCF electrode are larger than that of S/HKC. even at a high C-rate of 5C, the values of U_1 and Q_2/Q_1 of S/CHPCF electrode can still achieve as high as 2.24 V and 2.48, while the relevant values of C/HKC electrode are only 2.15 V and 2.28. Hence, we can deduce that both interfacial kinetics and Li^+/e transportation for S/CHPCF electrode are superior to that of S/HKC electrode. Those results together highlight the merits of CHPCF:1) the ordered 1D nanofibers and the cross-linking branches would provide high electrons transport pathway, which decrease the ohmic resistance by diminishing the contact resistance between the nanofibers; 2) the interconnected hierarchical pores offers "green channel" for electrolyte infiltration and Li^+ transportation. In this regard, the enhanced interfacial kinetics and Li^+/e^- transportation can well explain why the Li-S battery assembled with S/CHPCF electrode present excellent C-rate performance.

Both merits mentioned above were further investigated by the EIS method and quantitatively analyzed with equivalent circuit. As shown in Fig. 7a, it can be clearly seen that both EIS spectra are composed of a semicircle in the high frequency and a short line in the low frequency, representing the charge–transfer resistance (R_{ct}) and Warburg impedance.[47, 48] The R_{ct} can reflect the resistance of the electrochemical reaction at the boundary of electrode-electrolyte and the Warburg impedance is responded to Li^+ diffusion into the bulk of the materials.[47] In the equivalent circuit, R_s represents the ohmic resistance, including e^- and ions conductivity, R_{ct} is charge–transfer resistance of electrochemical reactions, CPE arises from double-layer capacitance and Wo is the Warburg impedance. The results were collected and exhibited in Fig. 7c. As can be seen, ohmic resistance (Rs) and Rct of the cell assembled with S/CHPCF electrode are 1.60 Ω cm^{-2} and 12.03 Ω cm^{-2}, which are only nearly 1/5 and 2/3 of the cell assembled with S/HKC electrode (Rs:7.59 Ω cm^{-2}, Rct:17.87 Ω cm^{-2}), respectively. The results further verified the high electrochemical activity and premium properties in Li^+/e transportation.

The high intrinsic electronic conductivity of CHPCF and S/CHPCF composites were further testified using a self-designed instrument as illustrated in Fig. 7d. As can be seen, the CHPCF shows a high electronic conductivity of 0.14 S cm^{-2}, which is nearly 4 folds of HKC (0.04 S cm^{-2}). Even though it dropped deeply after sulfur impregnation, electronic conductivitie of the S/CHPCF composite is still higher than S/HKC (S/CHPCF:0.035 S cm^{-2}, S/HKC: 0.01 S cm^{-2}, Fig. 7e). The electronic conductivity test provided a direct evidence to further highlights the merits in e^- transportation for the " through fiber jointing" electron transfer model of CHPCF.

To further quantify the difference of Li^+ diffusion in S/HKC and S/CHPCF electrodes, the diffusion coefficient of Li^+ (D) was calculated according to the following equation: [49, 50]

$$D = 0.5(RT / An^2F^2\sigma C)^2 \quad (3)$$

Where R is the ideal gas content, T is the absolute temperature, A is the geometrical area of the electrode surface, n is the number of electrons per molecule during oxidation, F is the Faraday's constant, C is the molar concentration of Li^+ and σ is the Warburg coefficient, which has a relationship with the real part of EIS spectra (Z') as follows:

$$Z' = Rs + Rct + \sigma\omega^{-1/2} \quad (4)$$

Where Rs, Rct and ω are ohmic resistance, charge–transfer resistance and angle frequency, respectively. The relationships between Z' and $\omega^{-1/2}$ in the low frequency of the two samples were listed in Fig. 7b. As can be seen, both curves show a linear characteristic in the selected region and the slope of the fitting line is σ, which together with D are listed in Fig. 7c. The S/CHPCF cathode shows an ion diffusion coefficient of 8.59 × 10^{-10} cm^2 s^{-1}, which is nearly two times of S/HKC electrode (4.52 × 10^{-10} cm^2 s^{-1}). The increased ion diffusion coefficient can be mainly attributed to the shorter diffusion path in the S/CHPCF electrode, due to the smaller size and excellent electrolyte-holding properties of the porous construct.[47] The results are highly consisted with the C-rate performance.

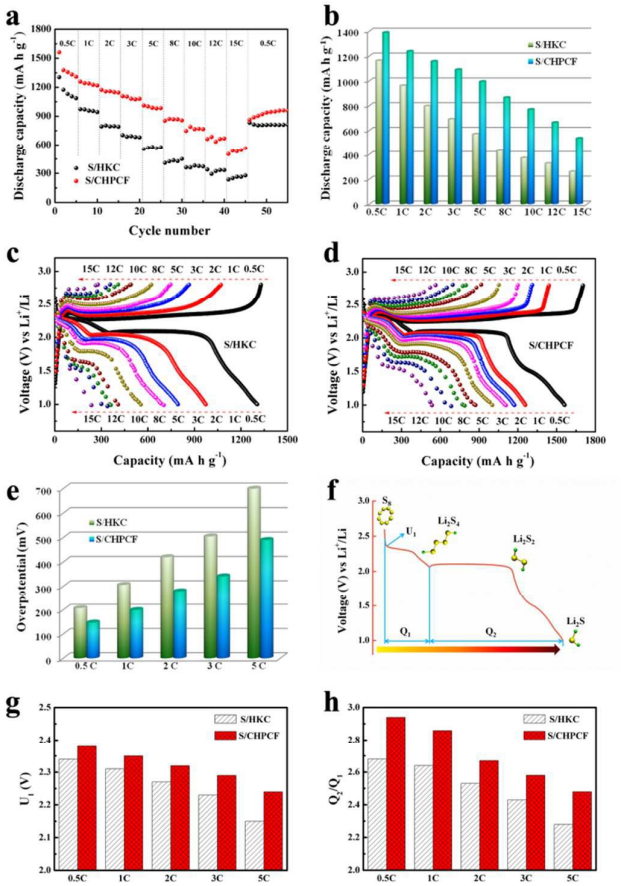

Fig. 6. Electrochemical properties of the S/HKC and S/CHPCF electrodes. (a) and (b) C-rate performance for S/HKC and S/CHPCF cathodes at various C-rate from 0.5C to 15C. Charge/discharge profiles for (c) S/HKC and (d) S/CHPCF at various C-rate from 0.5C to 15C. (e) Overpotential of S/HKC and S/CHPCF cathodes at various C-rate from 0.5C to 5C. (f) Schematic illustration of a typical voltage profile. (g) U_1 and (h) Q_2/Q_1 of S/HKC and S/CHPCF cathodes at various C-rate from 0.5C to 5C (data are collected from c-d).

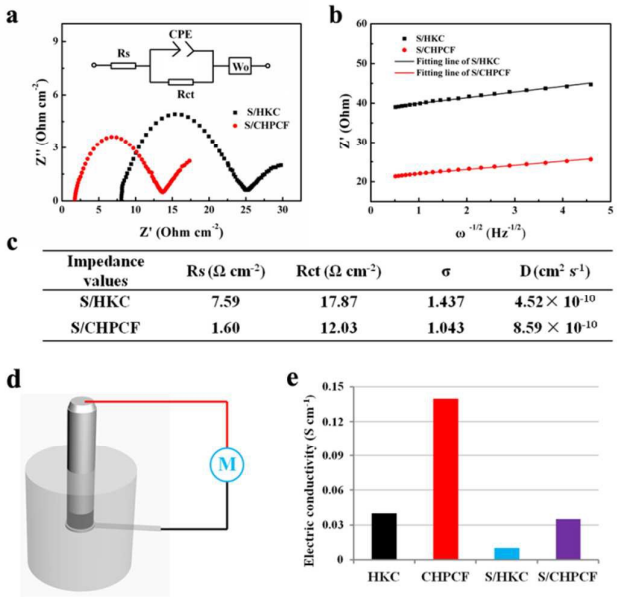

c

Impedance values	Rs (Ω cm^{-2})	Rct (Ω cm^{-2})	σ	D (cm^2 s^{-1})
S/HKC	7.59	17.87	1.437	4.52×10^{-10}
S/CHPCF	1.60	12.03	1.043	8.59×10^{-10}

Fig. 7. (a) EIS plots of the S/HKC and S/CHPCF electrodes before cycling. Inset is the used equivalent circuit. (b) Relationship between Z' and square root of frequency ($\omega^{-1/2}$) in the low-frequency region. (c) Kinetic parameters of S/HKC and S/CHPCF electrodes. (d) A self-designed electrical conductivity measurement. (e) Electrical conductivity of HKC, CHPCF, S/HKC and S/CHPCF composites.

To further evaluate its potential for practical application, Fig. S10a shows the C-rate performance of S/CHPCF electrode operated under low-temperatures, where the C-rate performance deteriorated seriously under low operating temperatures. Due to the week correlation between the temperature and electron conductivity for carbon materials, the main reason that causes the poor C-rate performance can be ascribed to the decreased rate of Li^+ transportation. Besides the factor that the increased electrolyte viscosity hindered the ion transport have been reported,[51] we also investigated the relationship between the ion conductivity and temperature, as shown in Fig. S10b, finding that the ion conductivity has a linear relationship with the temperature. When the temperature ranged from 25 °C to -20 °C, the ion conductivity decreased from 10.35 mS cm^{-1} to 4.52 mS cm^{-1}. Even though the ion transportation was strongly limited by electrolyte viscosity and ion conductivity under a low operating temperature, the Li-S batteries can still achieve a capacity as high as 515 mA h g^{-1} at 5C under 0 °C. Unfortunately, if further increasing C-rate or decreasing temperature (for example, -20 °C), the battery performance will drop down sharply and some self-heating technique might be considered for practical application. The S/CHPCF electrodes with higher active mass loadings were also used to evaluate the potential practical application of the cell. As presented in Fig. S11,when the mass loading was increased to 1.0 mg cm^{-2} and 1.7 mg cm^{-2}, high capacities of 615 mA h g^{-1} and 651 mA h g^{-1} were still obtained at 5C and 3C, respectively, which were among the state-of-art values ever reported.[8, 20, 25, 52] Besides that, as shown in Fig. 8, the soft package (geometric area: 77 × 50 mm^2) using the S/CHPCF electrode with 1.7 mg cm^{-2} could simply light up a logo as "DNL 17" that was composed of nearly 50 blue LED lights, and batteries of 300 Wh kg^{-1} (calculated based on coating 1.7 mg cm^{-2} sulfur on the both sides of current collector) could be achieved based on our calculation to assemble a soft package battery,[20] further proving its potential for practical application.

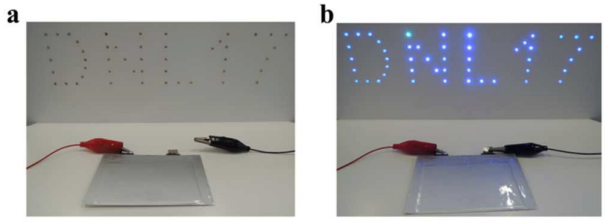

Fig. 8. The optical images show a blue LED logo (a) before and (b) after lit by a soft package Li–S battery assembled with S/CHPCF electrode.

Conclusion

A novel ordered cross-linking fibrous hierarchical porous carbon with 1D orientation derived from a Cu-MOF was well-designed for advanced Li-S batteries. The cross-linking structure between the carbon fibers enables fast (direct) electron transfer "through fiber jointing", instead of the traditional "through point contacting" between the contacted carbon units. The hierarchical porous distribution orderly ranged from below 2 nm to over 2 um size can tightly confine the soluble PS as well as supply Li^+ with "green channel", and further provide large space for electrolyte and sulfur accommodation. In this regard, the Li-S batteries assembled with S/CHPCF electrode exhibit good C-rate performance, such as the low capacity attenuation rate of 0.076% per cycle at 5C during 500 cycles as well as an outstanding high-rate capability of 534 mA h g^{-1} at 15C under room temperature. Additionally, still a high capacity of 515 mA h g^{-1} at 5C was attained under such a low operating temperature as 0 °C. In summary, this work provides a strategy to prepare a kind of carbon that can simultaneously meet the demand of Li^+ and e^- transport at high C-rates. It would arouse the great interest in other advanced high C-rate energy storage such as Li-O_2 batteries and supercapacitors.

Acknowledgements

The authors acknowledge financial support from National Natural Science Foundation of China (No. 51403209, 21406221, 51177156/E0712), Youth Innovation Promotion Association (CAS), 100 Talents Program of Dalian Institute of Chemical Physics, Natural Sciences Foundation of Liaoning Province of China (2013020126), Hubei Province-Chinese Academy of Sciences Cooperative Project.

Notes and references

1. P. G. Bruce, S. A. Freunberger, L. J. Hardwick and J. M. Tarascon, *Nat. Mater.*, 2012, **11**, 19-29.
2. W. Zhou, Y. Yu, H. Chen, F. J. DiSalvo and H. D. Abruña, *J. Am. Chem. Soc.*, 2013, **135**, 16736-16743.
3. B. Zhang, X. Qin, G. R. Li and X. P. Gao, *Energy Environ. Sci.*, 2010, **3**, 1531.

4. W. Li, Z. Liang, Z. Lu, H. Yao, Z. W. Seh, K. Yan, G. Zheng and Y. Cui, Adv. Energy Mater., 2015, DOI: 10.1002/aenm.201500211.

5. X. Ji, K. T. Lee and L. F. Nazar, *Nat. Mater.*, 2009, **8**, 500-506.
6. S. Waluś, C. Barchasz, R. Bouchet, J.-C. Leprêtre, J.-F. Colin, J.-F. Martin, E. Elkaïm, C. Baehtz and F. Alloin, *Adv. Energy Mater.*, **2015**, DOI: 10.1002/aenm.201500165.
7. Q. Zhao, X. Hu, K. Zhang, N. Zhang, Y. Hu and J. Chen, *Nano Lett.*, 2015, **15**, 721-726.
8. L. Ji, M. Rao, S. Aloni, L. Wang, E. J. Cairns and Y. Zhang, *Energy Environ. Sci.*, 2011, **4**, 5053.
9. G. Zhou, S. Pei, L. Li, D. W. Wang, S. Wang, K. Huang, L. C. Yin, F. Li and H. M. Cheng, *Adv. Mater.*, 2014, **26**, 625-631, 664.
10. R. Elazari, G. Salitra, A. Garsuch, A. Panchenko and D. Aurbach, *Adv. Mater.*, 2011, **23**, 5641-5644.
11. X. Ji and L. F. Nazar, *J. Mater. Chem.*, 2010, **20**, 9821.
12. S. Zhang, K. Ueno, K. Dokko and M. Watanabe, *Adv. Energy Mater.*, 2015, DOI: 10.1002/aenm.201500117.
13. Z. Wei Seh, W. Li, J. J. Cha, G. Zheng, Y. Yang, M. T. McDowell, P.-C. Hsu and Y. Cui, *Nat. Commun.*, 2013, **4**, 1331.
14. C. Liang, N. J. Dudney and J. Y. Howe, *Chem. Mater.*, 2009, **21**, 4724-4730.
15. X. Liang, Y. Liu, Z. Wen, L. Huang, X. Wang and H. Zhang, *J. Power Sources*, 2011, **196**, 6951-6955.
16. L. Yu, N. Brun, K. Sakaushi, J. Eckert and M. M. Titirici, *Carbon*, 2013, **61**, 245-253.
17. S. Xin, L. Gu, N. H. Zhao, Y. X. Yin, L. J. Zhou, Y. G. Guo and L. J. Wan, *J. Am. Chem. Soc.*, 2012, **134**, 18510-18513.
18. B. Guo, T. Ben, Z. Bi, G. M. Veith, X. G. Sun, S. Qiu and S. Dai, *Chem. Commun. (Camb)*, 2013, **49**, 4905-4907.
19. N. Brun, K. Sakaushi, L. Yu, L. Giebeler, J. Eckert and M. M. Titirici, *Phys. Chem. Chem. Phy.s*, 2013, **15**, 6080-6087.
20. Q. Li, Z. Zhang, Z. Guo, Y. Lai, K. Zhang and J. Li, *Carbon*, 2014, **78**, 1-9.
21. Y. Zhao, W. Wu, J. Li, Z. Xu and L. Guan, *Adv. Mater.*, 2014, **26**, 5113-5118.
22. J. Zhou, R. Li, X. Fan, Y. Chen, R. Han, W. Li, J. Zheng, B. Wang and X. Li, *Energy Environ. Sci.*, 2014, **7**, 2715.
23. C. Xu, Y. Wu, X. Zhao, X. Wang, G. Du, J. Zhang and J. Tu, *J. Power Sources*, 2015, **275**, 22-25.
24. Y. Dong, S. Liu, Z. Wang, Y. Liu, Z. Zhao and J. Qiu, *Nanoscale*, 2015, **7**, 7569-7573.
25. J. T. Lee, Y. Zhao, S. Thieme, H. Kim, M. Oschatz, L. Borchardt, A. Magasinski, W. I. Cho, S. Kaskel and G. Yushin, *Adv. Mater.*, 2013, **25**, 4573-4579.
26. X. Li, Q. Sun, J. Liu, B. Xiao, R. Li and X. Sun, *J. Power Sources*, 2016, **302**, 174-179.
27. P. Strubel, S. Thieme, T. Biemelt, A. Helmer, M. Oschatz, J. Brückner, H. Althues and S. Kaskel, *Adv. Funct. Mater.*, 2015, **25**, 287-297.
28. M. Wang, H. Zhang, Q. Wang, C. Qu, X. Li and H. Zhang, *ACS Appl. Mater. Interfaces*, 2015, **7**, 3590-3599.
29. Y. Ma, H. Zhang, B. Wu, M. Wang, X. Li and H. Zhang, *Sci. Rep.*, 2015, **5**, 14949.
30. Q. Sun, X. Fang, W. Weng, J. Deng, P. Chen, J. Ren, G. Guan, M. Wang and H. Peng, *Angew. Chem. Int .Ed.*, 2015, **127**, 1-7.
31. Y. Zhang, Y. Zhao, Z. Bakenov, M. R. Babaa, A. Konarov, C. Ding and P. Chen, *J. Electrochem. Soc.*, 2013, **160**, A1194-A1198.
32. S. J. Yang, M. Antonietti and N. Fechler, *J. Am. Chem. Soc.*, 2015, **137**, 8269-8273.
33. X. Yang, N. Yan, W. Zhou, H. Zhang, X. Li and H. Zhang, *J. Mater. Chem. A*, 2015, **3**, 15314-15323.
34. Y.-K. Seo, G. Hundal, I. T. Jang, Y. K. Hwang, C.-H. Jun and J.-S. Chang, *Microporous and Mesoporous Mater.*, 2009, **119**, 331-337.
35. S. S.-Y. Chui, S. M.-F. Lo, J. P. H. Charmant, A. G. Orpen and I. D. Williams, *Science* 1999, **283**, 1148-1150.
36. N. Dadgostar, S. Ferdous and D. Henneke, *Mater. Lett.*, 2010, **64**, 45-48.
37. Z. Cheng, H. Zhong, J. Xu, X. Chu, Y. Song, M. Xu and H. Huang, *Mater. Lett.*, 2011, **65**, 3005-3008.
38. G. Xu, B. Ding, L. Shen, P. Nie, J. Han and X. Zhang, *J. Mater. Chem. A*, 2013, **1**, 4490.
39. L. Wang, Y. Zhao, M. L. Thomas and H. R. Byon, *Adv. Funct. Mater.*, 2014, **24**, 2248-2252.
40. X. Yang, B. Dong, H. Zhang, R. Ge, Y. Gao and H. Zhang, *RSC Adv.*, 2015, **5**, 86137–86143 |.
41. H. Wang, Y. Yang, Y. Liang, J. T. Robinson, Y. Li, A. Jackson, Y. Cui and H. Dai, *Nano. Lett.*, 2011, **11**, 2644-2647.
42. G. Zheng, Y. Yang, J. J. Cha, S. S. Hong and Y. Cui, *Nano. Lett.*, 2011, **11**, 4462-4467.
43. K. Xi, S. Cao, X. Peng, C. Ducati, R. V. Kumar and A. K. Cheetham, *Chem. Commun. (Camb)*, 2013, **49**, 2192-2194.
44. W. Xia, B. Qiu, D. Xia and R. Zou, *Sci. Rep.*, 2013, **3**, 1935.
45. H. B. Wu, S. Wei, L. Zhang, R. Xu, H. H. Hng and X. W. Lou, *Chem. Eur. J.*, 2013, **19**, 10804-10808.
46. X. Liang, C. Hart, Q. Pang, A. Garsuch, T. Weiss and L. F. Nazar, *Nat. Commun.*, 2015, **6**, 5682.
47. M. Kazazi, M. R. Vaezi and A. Kazemzadeh, *Ionics*, 2013, **20**, 635-643.
48. W. G. Wang, X. Wang, L. Y. Tian, Y. L. Wang and S. H. Ye, *J. Mater. Chem. A*, 2014, **2**, 4316-4323.
49. Y. Yang, W. Xu, R. Guo, L. Liu, S. Wang, D. Xie and Y. Wan, *J. Power Sources*, 2014, **269**, 15-23.
50. Y. Cheng, K. Feng, W. Zhou, H. Zhang, X. Li and H. Zhang, *Dalton Trans*, 2015, **44**, 17579-17586.
51. S. Xiong, K. Xie and X. Hong, *Journal of National University of Defense Technology*, 2012, **34**, 150-154.
52. N. Nakamura, T. Yokoshima, H. Nara, T. Momma and T. Osaka, *J. Power Sources*, 2015, **274**, 1263-1266.

Graphical Abstract

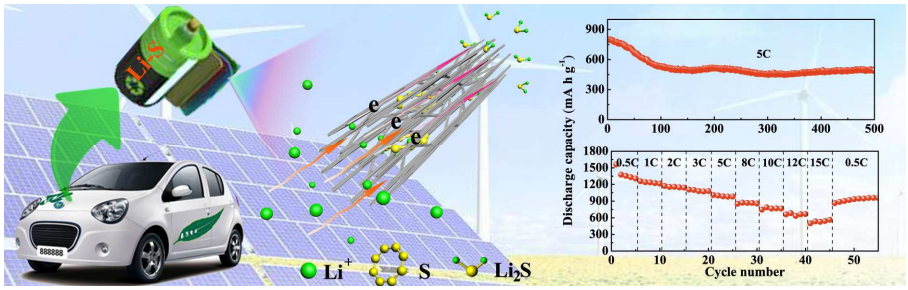

1-D oriented ordered cross-linking hierarchical porous carbon fibers were fabricated successfully. The prepared cross-linking hierarchical porous carbon fibers (CHPCF) as sulfur immobilizer demonstrated excellent cycling stability and high C-rate performance in Li-S batteries.